J Neurophysiol 89: 3279–3293, 2003.
First published March 20, 2003; 10.1152/jn.00242.2003.

Adaptation and Temporal Decorrelation by Single Neurons in the Primary Visual Cortex

Xiao-Jing Wang,[1] Yinghui Liu,[1] Maria V. Sanchez-Vives,[2] and David A. McCormick[3]

[1]*Volen Center for Complex Systems, Brandeis University, Waltham, Massachusetts 02454;* [2]*Instituto de Neurociencias, Universidad Miguel Hernandez-Consejo Superior de Investigaciones Cientificas, San Juan de Alicante, Spain; and* [3]*Department of Neurobiology, Yale University School of Medicine, New Haven, Connecticut 06510*

Submitted 28 May 2002; accepted in final form 15 November 2002

Wang, Xiao-Jing, Yinghui Liu, Maria V. Sanchez-Vives, and David A. McCormick. Adaptation and temporal decorrelation by single neurons in the primary visual cortex. *J Neurophysiol* 89: 3279–3293, 2003. First published March 20, 2003; 10.1152/jn.00242.2003. Limiting redundancy in the real-world sensory inputs is of obvious benefit for efficient neural coding, but little is known about how this may be accomplished by biophysical neural mechanisms. One possible cellular mechanism is through adaptation to relatively constant inputs. Recent investigations in primary visual (V1) cortical neurons have demonstrated that adaptation to prolonged changes in stimulus contrast is mediated in part through intrinsic ionic currents, a Ca^{2+}-activated K^+ current (I_{KCa}) and especially a Na^+-activated K^+ current (I_{KNa}). The present study was designed to test the hypothesis that the activation of adaptation ionic currents may provide a cellular mechanism for temporal decorrelation in V1. A conductance-based neuron model was simulated, which included an I_{KCa} and an I_{KNa}. We show that the model neuron reproduces the adaptive behavior of V1 neurons in response to high contrast inputs. When the stimulus is stochastic with $1/f^2$ or $1/f$-type temporal correlations, these autocorrelations are greatly reduced in the output spike train of the model neuron. The I_{KCa} is effective at reducing positive temporal correlations at approximately 100-ms time scale, while a slower adaptation mediated by I_{KNa} is effective in reducing temporal correlations over the range of 1–20 s. Intracellular injection of stochastic currents into layer 2/3 and 4 (pyramidal and stellate) neurons in ferret primary visual cortical slices revealed neuronal responses that exhibited temporal decorrelation in similarity with the model. Enhancing the slow afterhyperpolarization resulted in a strengthening of the decorrelation effect. These results demonstrate the intrinsic membrane properties of neocortical neurons provide a mechanism for decorrelation of sensory inputs.

INTRODUCTION

In natural environments, sensory inputs from the external world to the brain are statistically redundant, characterized by strong and long-range correlations in space (Ruderman 1994; Ruderman and Bialek 1994) and in time (Doug and Atick 1995a; van Hateren and van der Schaaf 1996). For the brain to encode sensory stimuli and detect changes efficiently, it is desirable to reduce input redundancy through a decorrelation operation (Atick 1992; Attneave 1954; Barlow 1961; Barlow and Foldiak 1989; Field 1994; Srinivasan et al. 1982). In the visual system, theoretical models, natural scene analysis, and physiological studies have shown that decreases of redundancy by decorrelation is key to the efficient neural encoding of images (Bell and Sejnowski 1997; Dan et al. 1996; Dong and Atick 1995b; Laughlin 1981; Olshausen and Field 1996; Vinji and Gallant 2000. For a review, see Simoncelli and Olshausen 2001). Barlow (1961, 1990) suggested that decorrelation could be subserved by neuronal adaptation in the neocortex. This idea is supported by recent work demonstrating that neuronal adaptation occurs over a wide range of time scales (Fairhall et al. 2001) and that these adaptation dynamics can serve to maximize information transmission (Baddeley et al. 1997; Brenner et al. 2000; Wainwright 1999). It is thus of considerable interest to identify cellular and synaptic mechanisms of adaptation and to investigate whether the same mechanisms can also subserve decorrelation in the brain.

In the primary visual cortex (V1), a neuron's response to a low-contrast visual pattern is substantially reduced (adapted) following a few seconds of stimulation (Ahmed et al. 1997; Blackmore and Campbell 1969; Carandini et al. 1998; Dragoi et al. 2000; Greenlee and Heitger 1988; Greenlee et al. 1991; Maffei et al. 1973; Movshon and Lennie 1979; Nelson 1991; Ohzawa et al. 1985; Sclar et al. 1985; Vidyasagar 1990). This history-dependent adaptive gain control allows visual cortical neurons to display a high sensitivity without being limited by saturation or insensitivity. In addition, pattern adaptation provides a mechanism to reduce redundancy in the processing of natural scenes—by removing temporally constant stimuli while remaining responsive to more rapid changes. Several mechanisms have been proposed for contrast adaptation of V1 neurons, including a slow form of synaptic depression (time constant: 10 s) (Adorján et al. 1999; Chance et al. 1998; Finlayson and Cynader 1995). Recent studies with intracellular recordings of cat primary visual cortical neurons in vivo revealed that prolonged (tens of seconds) presentation of optimal high-contrast visual stimuli results in a hyperpolarization of the recorded cell (Carandini and Ferster 1997; Sanchez-Vives et al. 2000a). This hyperpolarization correlates with the persistent decrease in sensitivity following adaptation and appears to be generated through ionic mechanisms intrinsic to single neurons. For example, intracellular current injection into single cortical cells could replicate the hyperpolarization induced by high-contrast visual stimuli (Sanchez-Vives et al. 2000a). Ex-

Address for reprint requests: X.-J. Wang, Center for Complex Systems, MS 013, Brandeis University, Waltham 02454 (e-mail: xjwang@brandeis.edu).

The costs of publication of this article were defrayed in part by the payment of page charges. The article must therefore be hereby marked "*advertisement*" in accordance with 18 U.S.C. Section 1734 solely to indicate this fact.

amination of similar hyperpolarizations generated in response to prolonged action potential activity in vitro reveal that it is generated by a Ca^{2+}-activated K^+ current I_{KCa} and especially a Na^+-activated K^+ current I_{KNa} (Sanchez-Vives et al. 2000b).

Based on these data, we constructed a conductance-based model of a visual cortical neuron endowed with I_{KCa} and I_{KNa}. The model was calibrated by reproducing the adaptive neural response to long-lasting sinusoidal currents (Sanchez-Vives et al. 2000b). Using correlated stochastic inputs (with 2nd-order statistics of natural scenes), we show that adaptation currents endow the model neuron with the ability to remove long-range temporal correlations in the input so that the output spike discharges are decorrelated at long time scales. Applying the same protocol of stochastic inputs to V1 cells in cortical slices, we found that neurons of primary visual cortex can indeed remove long-range temporal correlations in the stochastic inputs. Furthermore, an enhancement of the slow hyperpolarization in single cells increased the degree of decorrelation. These results suggest that intrinsic adaptation ionic currents provide a candidate cellular mechanism for temporal decorrelation in V1 neurons.

METHODS

The model

We were primarily motivated by the observation that slow membrane hyperpolarization resulting from repetitive activation of cortical neurons is largely produced by sodium/calcium-dependent potassium currents (Sanchez-Vives et al. 2000a,b). Here we implemented both types of adaptation currents in a Hodgkin-Huxley-type conductance-based model (Hodgkin and Huxley 1952). The model was modified from Wang (1998) with the addition of a sodium-activated potassium current I_{KNa}. The model has two compartments, one representing the soma/axonal initial segment (V_s), the other representing the dendrite (V_d) (Pinsky and Rinzel 1994). The spike-generating Na^+ and K^+ currents are located in the somatic compartment. High-threshold Ca^{2+} currents I_{Ca} are distributed in both compartments and activate Ca^{2+}-dependent K^+ currents I_{KCa}. A slow Na^+-activated K^+ current I_{KNa} is located in the somatic compartment.

The model obeys the following seven differential equations

$$C_m \frac{dV_s}{dt} = -I_L - I_{Na} - I_K - I_{Ca,s} - I_{KCa,s} - I_{KNa} - (g_c/p)(V_s - V_d) + I \quad (1)$$

$$\frac{dh}{dt} = \phi_h[\alpha_h(V_s)(1 - h) - \beta_h(V_s)h] \quad (2)$$

$$\frac{dn}{dt} = \phi_n[\alpha_n(V_s)(1 - n) - \beta_n(V_s)n] \quad (3)$$

$$\frac{d[Ca^{2+}]_s}{dt} = -\alpha_{Ca,s}I_{Ca,s} - [Ca^{2+}]_s/\tau_{Ca,s} \quad (4)$$

$$\frac{d[Na^+]_i}{dt} = -\alpha_{Na}I_{Na} - 3R_{pump}[\varphi_{Na}([Na^+]_i) - \varphi_{Na}([Na^+]_{eq})] \quad (5)$$

$$C_m \frac{dV_d}{dt} = -I_L - I_{Ca,d} - I_{KCa,d} - (g_c/(1 - p))(V_d - V_s) \quad (6)$$

$$\frac{d[Ca^{2+}]_d}{dt} = -\alpha_{Ca,d}I_{Ca,d} - [Ca^{2+}]_d/\tau_{Ca,d} \quad (7)$$

where $C_m = 1\ \mu F/cm^2$, I is the applied current, and the leak current is $I_L = g_L(V - V_L)$. The coupling current between soma and dendrite is proportional to $(V_s - V_d)$, with coupling conductance $g_c = 2\ mS/cm^2$. The parameter p = (somatic area/total area) = 0.5. Maximum conductances $g_L = 0.1$, $g_{Na} = 45$, $g_K = 18$, $g_{Ca,s} = g_{Ca,d} = 1$, $g_{KCa,s} = g_{KCa,d} = 5$, $g_{KNa} = 5$ in mS/cm^2. The reversal potentials $V_L = -65$, $V_{Na} = +55$, $V_K = -80$, $V_{Ca} = +120$ in mV.

The voltage-dependent currents are described by the Hodgkin-Huxley formalism (Hodgkin and Huxley 1952). The dynamics of the gating variable x follows first-order kinetics

$$\frac{dx}{dt} = \phi_x[\alpha_x(V)(1 - x) - \beta_x(V)x)]$$

$$= \phi_x[x_\infty(V) - x]/\tau_x(V) \quad (8)$$

with $x_\infty(V) = \alpha_x(V)/[\alpha_x(V) + \beta_x(V)]$ as the steady-state value and $\tau_x(V) = 1/[\alpha_x(V) + \beta_x(V)]$ as the time constant, and ϕ_x is the temperature factor.

The sodium current in the somatic compartment is $I_{Na} = g_{Na}m_\infty^3(V_s)h(V_s - V_{Na})$. The fast activation variable m is replaced by its steady-state value $m_\infty(V_s)$ (given that τ_m is only a fraction of a millisecond): $m_\infty = \alpha_m/[\alpha_m + \beta_m]$ and $\alpha_m(V) = -0.1(V + 33)/\{\exp[-0.1(V + 33)] - 1\}$ and $\beta_m(V) = 4\exp[-(V + 58)/12]$. The inactivation variable h for I_{Na} is described by $\alpha_n(V) = 0.07\exp[-(V + 50)/10]$ and $\beta_h(V) = 1/\{\exp[-0.1(V + 20)] + 1\}$. The delayed rectifier is $I_K = g_K n^4(V_s - V_K)$, with the activation variable n described by $\alpha_n(V) = -0.01(V + 34)/\{\exp[-0.1(V + 34)] - 1\}$ and $\beta_n(V) = 0.125 \times \exp[-(V + 44)/25]$. The temperature factor $\phi_h = \phi_n = 4$.

The high-threshold calcium current $I_{Ca} = g_{Ca}v_\infty^2(V)(V - V_{Ca})$, where the activation variable v is replaced by its steady-state value $v_\infty(V) = 1/\{1 + \exp[-(V + 20)/9]\}$ because of its fast dynamics. The voltage-independent, calcium-activated potassium current $I_{KCa} = g_{KCa}([Ca^{2+}]_i/([Ca^{2+}]_i + K_D))(V - V_K)$, with $K_D = 30\ \mu M$. The intracellular calcium concentration $[Ca^{2+}]_i$ is assumed to be governed by a linear equation with α_{Ca} proportional to the ratio of the membrane area and the volume immediately beneath the membrane, $\alpha_{Ca} = 0.002\ \mu M\ (ms\mu A)^{-1}\ cm^2$ in the dendrite compartment and $0.00067\ \mu M\ (ms\mu A)^{-1}\ cm^2$ in the somatic compartment. The various extrusion and buffering mechanisms are described collectively by a first-order decay process with a time constant $\tau_{Ca} = 80$ ms in the dendritic compartment and 240 ms in the somatic compartment (Helmchen et al. 1996).

The Na^+-activated K^+ current I_{KNa} (Dryer 1994; Egan et al. 1992a,b; Kameyama et al. 1984; Schwindt et al. 1988, 1989) is modeled according to a quantitative study of this ionic current in dorsal root ganglion cells (Bischoff et al. 1998). The intracellular $[Na^+]_i$ concentration is incremented by Na^+ influx through I_{Na} during action potentials. (In cortical neurons, Na^+ influx could also be contributed by synaptic currents, which we do not model here for the sake of simplicity.) The Na^+-dependent K^+ current $I_{KNa} = g_{KNa}\omega_\infty([Na^+]_i)(V_s - V_K)$, with the activation function $\omega_\infty([Na^+]_i)$ given by (Bischoff et al. 1998)

$$\omega_\infty([Na^+]_i) = \frac{P_{max}}{1 + (EC_{50}/[Na^+]_i)^{n_H}} \quad (9)$$

where $P_{max} = 0.37$ defines the maximum opening probability of the channels. $EC_{50} = 38.7$ mM is the $[Na^+]_i$ for half activation and the Hill coefficient $n_H = 3.5$. The influx of $[Na^+]_i$ is controlled by $-\alpha_{Na} I_{Na}$. We chose $\alpha_{Na} = 0.0003$ mM $(ms\mu A)^{-1}$ cm^2 so that the influx of $[Na^+]_i$ is $\sim$100 μM per action potential. This number is consistent with the measurements using the Na^+-sensitive dye SBFI from hippocampal pyramidal neuron's soma and dendrites (Jaffe et al. 1992; Rose and Ransom 1997; Rose et al. 1999). Although SBFI imaging gives only relative changes rather than absolute Na^+ concentration, indirect estimates range from 50 to 300 μM/spike (Rose et al. 1999; W. N. Ross, personal communication).

The extrusion of $[Na^+]_i$ is assumed to be largely due to a Na^+/K^+ ionic pump, which extrudes three Na^+ ions for every two K^+ ions brought into the cell (Fain 1999). Previous in vitro studies (Sanchez-Vives et al. 2000a) show that the slow after-hyperpolarization following prolonged discharge is mediated largely by I_{KNa} with a relatively small or latent contribution by the Na^+/K^+ pump. Therefore here we have focused on the influence of I_{KNa} on temporal decorrelation and for simplicity have not included the current generated by the Na^+/K^+ pump. However, our conclusions would remain the same, if such a current is taken into account, because it has the same time course as I_{KNa}.

The $[Na^+]_i$ extrusion by the ion pump was modeled (Li et al. 1996) as $-3R_{pump}(\varphi_{Na}([Na^+]_i) - \varphi_{Na}([Na^+]_{eq})$ where $\varphi_{Na}(x) = x^3/(x^3 + K_p^3)$ with $K_p = 15$ mM. The cubic nonlinearity is related to the cooperative binding of three Na^+ ions to the pump molecule in the early steps of Na^+ transport. $R_{pump} = 0.0006$ mM/ms. The sodium concentration at the resting state is assumed to be $[Na^+]_{eq} = 8$ mM (Galvan et al. 1984; Grafe et al. 1982). The equilibration of $[Na^+]_i$ is a nonlinear process and takes tens of seconds. The very slow kinetics of the Na^+/K^+ ionic pump is important for the model to reproduce visual cortical neurons' slow adaptation behavior.

Model simulations were carried out on a PC Pentium computer, using the fourth-order Runge-Kutta integration method and a time step of 0.05 ms.

Temporally correlated input

The spatial-temporal power spectrum $S(k, f)$, where $k \sim 1/L$ is the spatial frequency and $f \sim 1/T$ is the temporal frequency, has been used to characterize the second-order statistics of natural scenes. Typically, the spatial power spectrum of a natural image behaves $\sim 1/k^2$ (Ruderman 1994). The temporal power spectrum scales like $1/f^2$ when observed with a broad visual field (at large L) and $1/f$ when observed with a narrow visual field (small L) (Dong and Atick 1995a; van Hateren 1997). The characteristic relationship between power and frequency reflect strong temporal-spatial correlations present in natural scenes. Both $1/f^2$ and $1/f$ type inputs were used in this study.

A temporally correlated stochastic input with $1/f^2$ type spectral scaling can be generated by an Ornstein-Uhlenbeck process as

$$\frac{dI}{dt} = -I/\tau_{corr} + \sigma\eta(t) \tag{10}$$

where the decay time constant is $\tau_{corr} = 2000$ ms, $\eta(t)$ is a Gaussian white-noise term, and σ is the standard deviation of the noise distribution. Note that the precise value of τ_{corr} is not important as long as it is large enough so that the power spectrum of the input has a reasonable range of $1/f^2$ scaling (see following text). The generated input $I(t)$ is a correlated stochastic process, its autocorrelation function is

$$\langle I(t)I(t+\tau)\rangle = (\sigma^2\tau_{corr}/2)\exp(-\tau/\tau_{corr}) \tag{11}$$

which shows a positive correlation with characteristic correlation range τ_{corr}. The power spectrum of $I(t)$ is

$$S_I = \frac{\sigma^2}{\omega^2 + (1/\tau_{corr})^2} \tag{12}$$

Therefore $S_I \sim \sigma^2/\omega^2$ for $1/\tau_{corr} \ll \omega$. Therefore, a good range of $1/f^2$ scaling can be realized for a sufficiently long τ_{corr}. The power reaches a plateau at very low frequencies $\omega < 1/\tau_{corr}$, or $f = \omega/2\pi < 1/(2\pi\tau_{corr}) \simeq 0.1$ Hz.

There is no simple stochastic differential equation for generating $1/f$-type inputs. Therefore we used another method, derived from an explicit $1/f$ power spectrum through the inverse Fourier transform

$$I(t) = \int \sqrt{S(f)}\ \xi(f) e^{i(tf+\phi_f)} df \tag{13}$$

where $S(f) \sim 1/f$ and $\xi(f)$ is a Gaussian white-noise term with a prescribed variance, and ϕ_f is a statistically independent random phase. By this construction, the power spectrum of $I(t)$ is $\langle(\sqrt{S(f)}\ \xi(f)e^{i\phi_f})^2\rangle = S(f)$. Experimental evidence indicates that the early stage of visual signal processing (such as a photoreceptor) acts as a low-pass filter and the power for frequencies >20–30 Hz is filtered out (van Hateren 1997). To mimic this in our model, we introduced a cutoff of [$S(f) = 0$ for $f > 20$ Hz].

Temporal correlation of the neuronal activity

A spike train is a point process described by a sequence of delta functions in time $s(t) = \Sigma_i \delta(t - t_i)$. One could calculate directly the autocorrelation function of this point process (Gabbiani and Koch 1998). However, to assess the decorrelation effect, we need to compare the time correlation of the output with that of the signal, which is an analog quantity. For this reason, we converted the discrete spike train into a continuous instantaneous rate function $r(t) = 1/(t_{i+1} - t_i)$ for $t_i < t < t_{i+1}$. The autocorrelation function for $r(t)$ is calculated, with normalization, as follows

$$\phi(\tau) = \frac{\int_{-\infty}^{+\infty} r(t)r(t+\tau)dt - (\int_{-\infty}^{+\infty} r(t)dt)^2}{\int_{-\infty}^{+\infty} r(t)^2 dt - (\int_{-\infty}^{+\infty} r(t)dt)^2} \tag{14}$$

with $\phi(-\tau) = \phi(\tau)$, $-1 \le \phi(\tau) \le 1$ and $\phi(\tau = 0) = 1$. The same formula is used to compute the autocorrelation function of the input current $I(t)$. Because both are normalized to 1 at $\tau = 0$, the input and output autocorrelations can be compared directly on the same graph.

The power spectrum density is calculated directly from long time series (time duration $T > 50$ s if $f_{min} = 1/T < 0.02$ Hz). We normalized the power spectrum so that its integral (the total power) is the same for the input and the output. This allowed the relative power at different frequencies in the input and output to be compared.

In vitro experimental work

To test the theoretical predictions, intracellular recordings were performed from layers 2/3 and 4 (pyramidal and spiny stellate) neurons in primary visual cortex slices from the ferret. Ferrets were cared for and used in accordance with all appropriate regulatory guidelines. For the preparation of slices, 2- to 4-month-old ferrets of either sex were deeply anesthetized with pentobarbital sodium (40 mg/kg) and killed by decapitation. The forebrain was rapidly removed, and the hemispheres were separated with a midline incision. Four-hundred-micrometers-thick coronal slices of the primary visual cortex were cut on a vibratome (DSK Microslicer; Ted Pella, Redding, CA). A modification of the technique developed by Aghajanian and Rasmussen (1989) was used to increase tissue viability. During preparation of slices, the tissue was placed in a solution in which NaCl was replaced with sucrose while maintaining an osmolarity of 307 mosM. After preparation, slices were placed in an interface style recording chamber (Fine Sciences Tools, Foster City, CA). Cortical slices were superfused for the first 10 min with an equal mixture by volume of the normal bathing medium and the sucrose-substituted solution. Following this, normal bathing medium was switched into the chamber throughout the experiment. Bath temperature was maintained at 34–35°C.

Intracellular recordings were initiated following 2 h of recovery. The normal bathing medium contained (in mM) 124 NaCl, 2.5 KCl, 2 $MgSO_4$, 1.25 $NaHPO_4$, 2 $CaCl_2$, 26 $NaHCO_3$, and 10 dextrose and was aerated with 95% O_2-5% CO_2 to a final pH of 7.4. Block of transmembrane Ca^{2+} currents was achieved by replacing $CaCl_2$ with either $MnCl_2$ or $CoCl_2$ while sodium phosphate was omitted from the bathing medium to avoid precipitation.

Sharp intracellular recording electrodes were formed on a Sutter Instruments (Novato, CA) P-80 micropipette puller from medium-walled glass (1BF100, WPI Sarasota, FL) and beveled on a Sutter Instruments beveller to final resistances of 50–100 MΩ. Micropipettes were filled with 2 M Kacetate. Only those cells that maintained a stable resting membrane potential and responded to depolarizing current injection with the generation of trains of action potentials were included for analysis. In addition to square current pulses and sinusoidal currents, correlated stochastic currents with either $1/f^2$ or $1/f$ statistics—the same inputs used in model simulations—were also injected into the recorded cells. Clampex 6.0 (Axon Instruments) was the software used to transform the numerical series into an injected current. For the purpose of this study, the size of the slow afterhyperpolarization in a cell was measured from responses to either current pulses or sinusoidal currents of long duration. The temporal correlations in the output spike trains were analyzed and compared with that of the injected waveform.

RESULTS

Adaptive response to high-low sinusoidal current input

We first calibrated our model by simulating intracellular data from visual cortical neurons (Sanchez-Vives et al. 2000b). To compare the model with data, we used the same low-high-low intensity pattern of 2-Hz sinusoidal injected current in the simulation as in the experiments (Fig. 1). The 2-Hz sinusoidal current input in the model has a mean of 2 $\mu A/cm^2$. The low-intensity input (with an amplitude of 0.3 $\mu A/cm^2$) is applied before and after the high-intensity input (amplitude of 3 $\mu A/cm^2$, duration of 20 s). The model cell generates two spikes per cycle with the low-intensity input before the high-intensity input. At the beginning of the high-intensity current, as many as nine spikes are generated during the first cycle. The steady state of four spikes per cycle is reached after slow adaptation (Fig. 1*B*). Following the high-intensity sinusoidal current, a prolonged slow afterhyperpolarization (sAHP) of ~10 s can be observed (Fig. 1*A*). These results are similar to those obtained with recordings of visual cortical neurons in vitro (Sanchez-Vives et al. 2000b). The effects of I_{KCa} and I_{KNa} are clearly different in the model. Because the decay time constant for $[Ca^{2+}]_i$ is only 80 and 240 ms (in the dendritic and somatic compartments) and each cycle is 500 ms long, $[Ca^{2+}]_i$ does not accumulate over cycles and I_{KCa} is effective as a feedback control mechanism only *within* a cycle (Fig. 1*D*). By contrast, I_{KNa} is much slower. During low-intensity sinusoidal stimulation, intracellular $[Na^+]_i$ has a steady state of ~14 mM (Fig. 1*C*). During high-intensity stimulation, $[Na^+]_i$ accumulates slowly to a plateau level of 17.5 mM. The time course is exponential with a time constant of $\tau_{adap} \simeq 4$ s. A qualitative derivation of τ_{adap} is given in the APPENDIX (see also Liu and Wang 2001; Wang 1998). The same exponential time course is seen for the decreasing instantaneous firing rate associated with adaptation (Fig. 1*B*), showing that the slow spike-frequency adaptation is caused by the increase of $[Na^+]_i$, hence I_{KNa}. The slow afterhyperpolarization following the high-intensity stimulation displays a similar time course as $[Na^+]_i$, and the decay of I_{KNa} controls the time course of the post-adaptation recovery of neuronal excitability. The decay time constant of sAHP is therefore governed by the slow kinetics of the Na^+/K^+ pump. When the $[Na^+]_i$ is around $[Na^+]_{eq} = 8$ mM, its decay through the ionic pump can be approximately linearized by $\varphi(Na) = \varphi(Na_{eq}) + \varphi'(Na_{eq})(Na - Na_{eq})$. The equation for $[Na^+]_i$ decay back to $[Na^+]_{eq}$ is approximately given by

$$\frac{d[Na^+]_i}{dt} = -3R_{pump}\varphi'([Na^+]_{eq})(Na - Na_{eq}) \quad (15)$$

which yields the decay time constant $\tau_{Na} = 1/(3R_{pump}\varphi'([Na^+]_{eq})) \simeq 13$ s.

Decorrelation of $1/f^2$-type inputs by intrinsic adaptation mechanisms

In response to a long-lasting constant input, the model neuron adapts over time and its firing activity is small in the steady state. On the other hand, because the slow I_{KNa} acts with a delay, rapid changes in the input cannot be filtered out and will be detected and encoded by vigorous transient neural responses. Therefore adaptation ion channels could provide a cellular mechanism to remove temporal redundancy in the input. To test this hypothesis, we used stochastic current injections with prescribed autocorrelation statistics (see METHODS). For a stochastic current generated from an Ornstein-Uhlenbeck process (decay time constant $\tau_{corr} = 2000$ ms), the power spectrum $\sim 1/\omega^2$ when $\omega \gg (1/\tau_{corr}) = 0.5$ Hz and reaches a plateau for small $\omega \ll (1/\tau_{corr})$ (Fig. 2). The cutoff frequency for the plateau is given by $\omega \simeq 1/\tau_{corr}$, or $f \simeq 1/(2\pi\tau_{corr}) \simeq 0.1$ Hz.

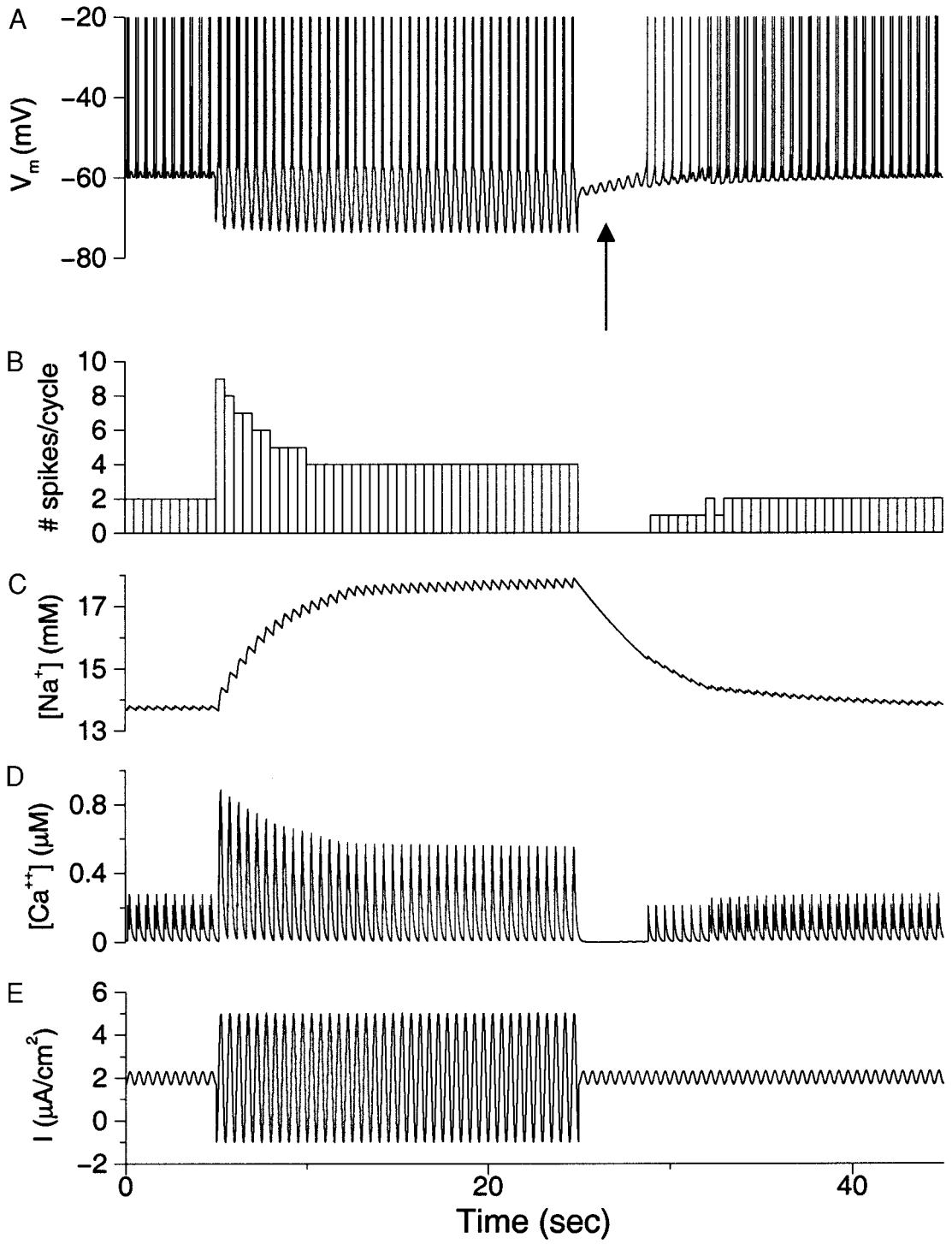

FIG. 1. Adaptation of the model neuron in response to a low-high-low sinusoidal current input. *A*: membrane potential. Following the injection of high-amplitude sinusoidal current there is a slow hyperpolarization lasting for ~10 s (arrow). *B*: number of spikes per cycle. *C*: intracellular $[Na^+]_i$ accumulation mirrors the adaptation time course of the instantaneous firing rate during the high-contrast input; whereas $[Na^+]_i$ decay is correlated with the slow hyperpolarization and recovery during the 2nd low-amplitude period. *D*: $[Ca^{2+}]_i$ decays fast back to the baseline between cycles. *E*: 2-Hz sinusoidal injected current that varies from low to high to low in amplitude. In this simulation, $g_{KNa} = 8$ mS/cm^2 and $g_{Ca,s} = 0$.

As shown in Fig. 2, in response to such a correlated stochastic current, the model neuron's spike activity is not a linear transformation of the input (Fig. 2*A*). Compared to the input, the output autocorrelation is suppressed at long time scales, and is zero for $\tau > 2$ s (Fig. 2*B*). The power spectrum shows a relative enhancement at high frequencies (>1 Hz). Concomitantly, there is a relative loss of power at low frequencies (<0.1 Hz), the plateau is reduced from 1.8 for the input to 0.5 for the output (Fig. 2*C*).

We noticed that decorrelation could occur even without

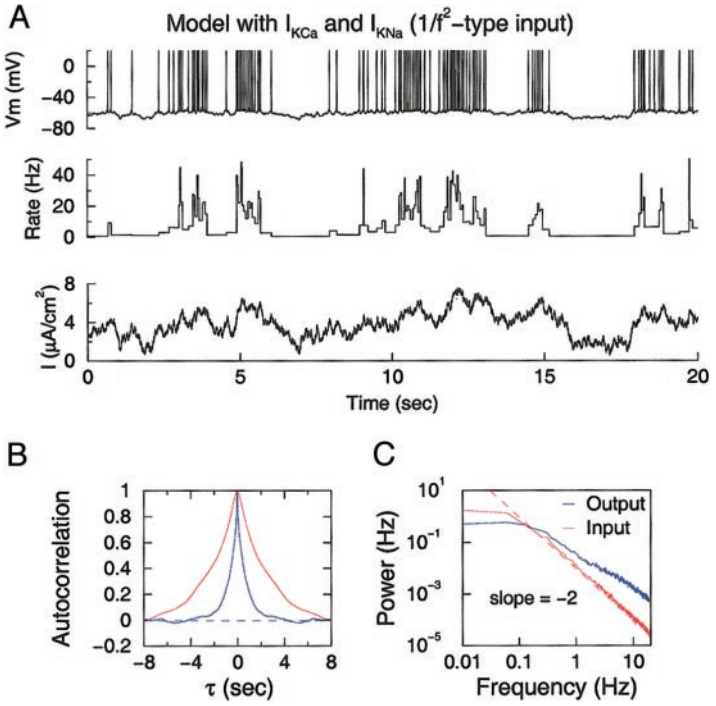

FIG. 2. Decorrelation of $1/f^2$-type stochastic inputs. *A*: membrane potential (*top*), instantaneous firing rate (*middle*), and input current (*bottom*). *B*: the autocorrelation function of the output is reduced compared to that of the input at all time scales and is essentially 0 for $\tau > 2$ s. *C*: power spectrum analysis for both the output and the input. The relative power for the output is reduced at low frequencies and enhanced at high frequencies.

adaptation currents if the model neuron fires at such a low rate that the spike discharges before and after a long silent episode could become statistically uncorrelated. We examined this effect by removal of the adaptation currents from the model cell. Replacing the adaptation currents with constant current injection revealed that obtaining decorrelation effects similar to those of the intact model (e.g., such as those illustrated in Fig. 2) required the average firing rate to be very low ($r < 1$–2 Hz; data not shown). Roughly speaking, to achieve significant decorrelations, the average interspike interval ($1/r$) should be comparable to, or longer than, the input correlation time (e.g., seconds in the present case). When the firing rate is reasonably high ($\geq$10 Hz), this effect cannot produce significant decorrelation of input.

In the presence of the slow adaptation currents I_{KCa} and I_{KNa}, the activation of I_{KNa} occurs in response to action potential activity as a slow negative feedback (as opposed to the constant injection of current) such that the occurrence of slow modulations of the membrane potential are decreased, whereas fast modulations are left intact. Thus the activation of adaptation currents in response to activity is more effective in reducing slow temporal correlations without destroying the fast responsiveness of the neuron (e.g., the membrane potential is "recentered" during slow changes as opposed to just simply constantly hyperpolarized). Maintained periods of depolarization and activity result in an increase in activation of the adaptation current therefore a reduction in excitability, whereas prolonged periods of hyperpolarization result in a de-activation of the adaptation currents and consequently an increase in neuronal responsiveness. Consequently, while without adaptation, the neuron's current threshold for spike discharges is 0.5 μA/cm^2, in the presence of slow adaptation (e.g., during periods of sustained current injection), the neuron do not fire all the time even though the average injected current ranges from 1 to 4 μA/cm^2 (Fig. 2*A*).

Decorrelation of 1/f-type inputs by I_{KCa} and I_{KNa} at separate time scales

In contrast to an $1/f^2$-type input generated by an Ornstein-Uhlenbeck process, an $1/f$-type input displays temporal correlations over arbitrarily long time scales: its autocorrelation is large over many seconds, and its power spectrum increases as $1/f$ at low frequencies (Fig. 3, *B* and *C*). The input shows very slow time modulations (Fig. 3*A*, *top*). Compared to Fig. 2, there is also larger fluctuations at high frequencies because the power decreases more slowly ($1/f$) than an $1/f^2$ input. In the absence of I_{KCa} and I_{KNa}, the model neuron transduces the input faithfully, the autocorrelation function and power spectrum of its spike train output is identical to those of the input (data not shown). Endowed with adaptation currents, the model neuron shows transient activity (Fig. 3*A*, *3rd panel*). The autocorrelation quickly decays to zero within 500 ms (Fig. 3*B*). Compared to the input, the output power spectrum shows a strong suppression at low frequencies. In effect, the output spectrum is flattened or "whitened" for $f < 0.1$ Hz, in contrast to the increases according to $1/f$ for the input (Fig. 3*C*). The transient nature of the neural activity is not simply due to a constant hyperpolarization but to time-dependent negative feedback. Compare for instance the two time windows indicated by horizontal bars, each lasting for 10 s (Fig. 3*A*, *top*). The second marked time window has a lower average "ambient" input current I than the first one. However, the first time window is preceded by a period of high activity and a large $[Na^+]_i$ plateau (hence a strong I_{KNa}), whereas the second time window follows a period of relative quiescence (Fig. 3*A*). As a result, the effective current input $I - I_{KNa}$ is larger, and the overall firing rate is actually slightly higher (8 Hz) during the second time window than that (7.6 Hz) during the first time window. Therefore, the slow changes in $[Na^+]_i$ track the input history over a period of seconds. The subsequent activation of I_{KNa} then acts as a negative feedback signal, the size of which

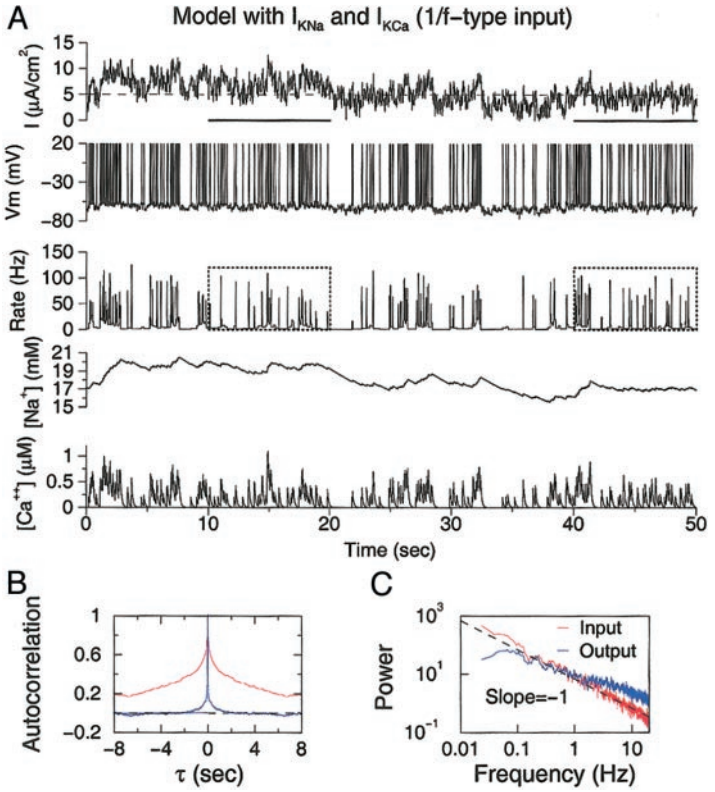

FIG. 3. Decorrelation of 1/*f*-type stochastic input. *A*: from *top* to *bottom:* input current, membrane potential, instantaneous firing rate, intracellular Na^+ and Ca^{2+}. Two time epoches (each lasting for 10 s) are indicated by boxes for the instantaneous firing rate (*3rd panel*). The 1st time window has a larger "baseline" input current I than the 2nd one (see - - -, *top*). However, $[Na^+]_i$ (hence I_{KNa}) is larger during the 1st time window due to a higher activity level that precedes the marked time window. As a result, the effective input current is $I - I_{KNa}$, and the average firing rate is actually lower in the 1st time window than in the 2nd one. *B*: autocorrelation functions for both the output and the input. The output is dramatically decorrelated both at short and long time scales, its autocorrelation is zero for $\tau > 2$ s. *C*: compared to the input, the power spectrum of the output is flattened (whitened) at low frequencies (<1 Hz).

is proportional to the time-averaged input in the recent past. The neuron becomes relatively insensitive to "ambient" input levels, yet still responds vigorously to transient input changes thanks to the lagged action of slow adaptation.

How large are the increases in membrane conductance that mediate these effects? An increase of the internal Na^+ from 17 to 20 mM in the model leads to an increase of g_{KNa} by 0.07 $\mu S/cm^2$, resulting in an increase in total resting membrane conductance of only 30%. Thus the temporal decorrelation occurs largely through slow changes in membrane potential (recentering) mediated by activation and de-activation of the adaptation currents and not through a "shunting" of the membrane.

We have examined the differential roles of I_{KCa} and I_{KNa} in the reduction of input redundancy. Without adaptation by either I_{KNa} or I_{KCa}, the output firing rate time course is nearly identical to the time course of the inject current (Fig. 4*A*). Addition of I_{KCa} alone leads to a suppression of the slow temporal modulation of the firing output compared to the input. This effect is significant only at moderate frequencies that

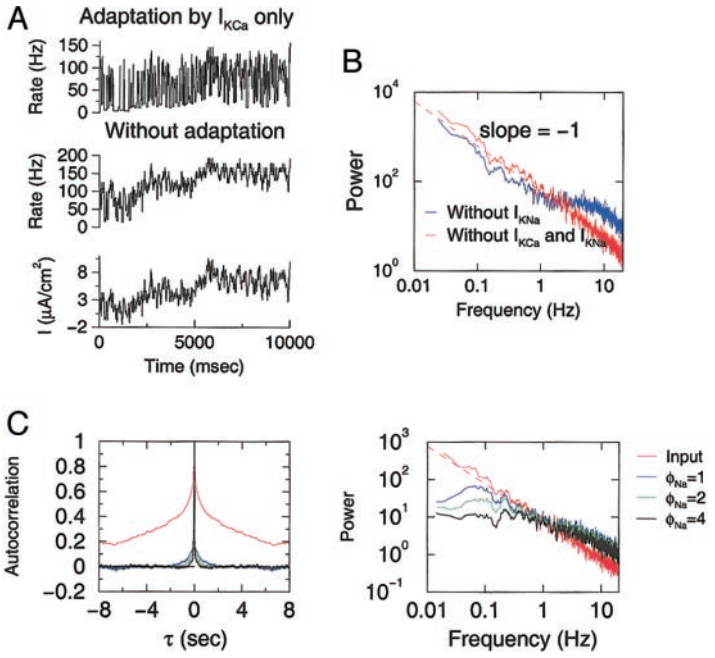

FIG. 4. Decorrelation at low frequencies (long time scales) critically depends on the I_{KNa}. *A* and *B*: I_{KNa} blockade. *A*: when both adaptation currents are blocked (*middle*), the neural firing output shows a similar slow time course as the input (*bottom*). I_{KCa} reduces this low-frequency modulation and enhances relative power of fluctuations at higher frequencies (*top*). *B*: the power spectrum calculated from output rate with and without I_{KCa} are superimposed. The flattening of the power spectrum due to temporal decorrelation by I_{KCa} is only limited to higher frequency range ~1–20 Hz. *C*: dependence of decorrelation on the speed of $[Na^+]_i$ kinetics (controlled by the parameter ϕ_{Na}). Faster $[Na^+]_i$ kinetics abolishes the autocorrelation at short temporal range (<2 s) more effectively (*left*) and whitens the power spectrum more strongly at <1 Hz (*right*).

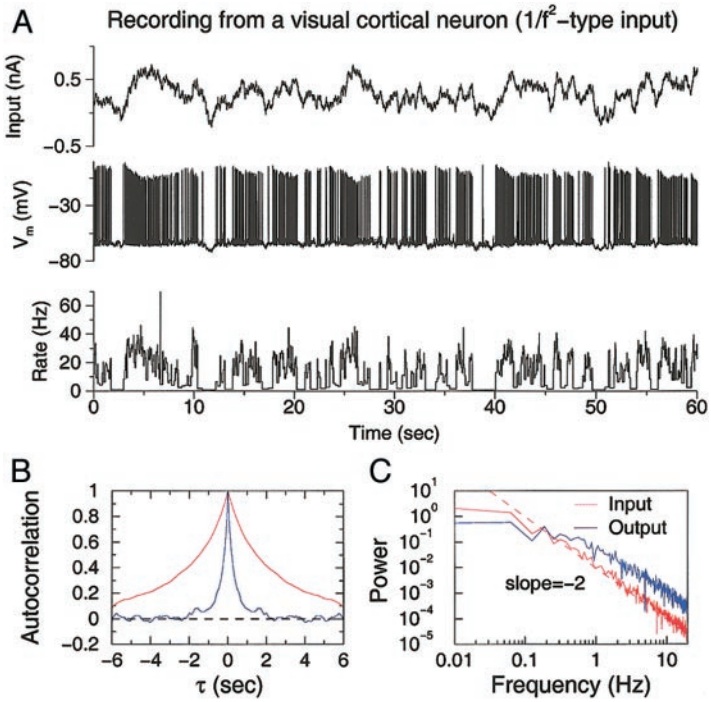

FIG. 5. In vitro intracellular recording from a visual cortical neuron ($1/f^2$ type input). *A*: top, injected current with $1/f^2$ type power spectrum; *middle*, recording of membrane potential; *bottom*, instantaneous firing rate. *B*: autocorrelation function for the input and the output. The output is significantly decorrelated at long time scales. *C*: power for the output is reduced in the low frequency range.

match the time scale of activation and deactivation of this current. This appeared as a "flattening" of the power-frequency relationship between 1 and ~10 Hz. At low (<1 Hz) frequencies, I_{KCa} is not persistent enough to influence interspike intervals, and therefore the power-frequency relationship has a similar shape as without I_{KCa} (see Fig. 4*B*). The relative power at 1–20 Hz is enhanced (Fig. 4*B*). At higher frequencies (>20 Hz), the rate of activation of I_{KCa} is too slow to have a significant effect on the firing temporal fluctuations. In the APPENDIX, we provide an analytical derivation to show that the relative enhancement of power at 1–20 Hz is due to a high-pass filtering of inputs by the adaptation current I_{KCa}.

The addition of I_{KNa} to the model results in a marked flattening of the power-frequency relationship at frequencies below ~1 Hz (Fig. 3). This effect is dependent upon the time scale of the $[Na^+]_i$ dynamics as demonstrated directly by accelerating the $[Na^+]_i$ kinetics with a scaling factor ϕ_{Na} (so that both the influx and extrusion are faster)

$$\frac{d[Na^+]_i}{dt} = \phi_{Na}(-\alpha_{Na} I_{Na} - 3R_{pump}(\varphi_{Na}([Na^+]_i) - \varphi_{Na}([Na^+]_{eq}))) \quad (16)$$

while all other parameters were maintained. As ϕ_{Na} is increased from 1 to 2 and 4, the temporal decorrelation by I_{KNa} at relatively short temporal ranges (<2 s) becomes more effective as shown in the autocorrelation function (Fig. 4*C*, *left*). The power spectrum shows stronger flattening (whitening) in the frequency range ≤1 Hz (Fig. 4*C*, *right*). The relative power at higher frequencies, however, remains unaffected.

Temporal decorrelation in visual cortical neurons

To test whether real cortical neurons can indeed decorrelate the inputs by intrinsic adaptation mechanisms, we used intracellular recordings from layer 2/3 pyramidal and layer 4 stellate neurons ($n = 32$) in ferret primary visual cortical slices. The injected stochastic currents are the same as those used in model simulations and possessed a prescribed long temporal correlations. Figure 5 shows an example with the $1/f^2$ type input (the Ornstein-Uhlenbeck process with a correlation time $\tau_{corr} = 2000$ ms). The baseline of the current was adjusted so that the neuron had an average firing rate ~10 Hz throughout each 60-s period of injected current. Although the recorded output exhibits some similarity with the input pattern, it is more transient in time (Fig. 5*A*). Temporal correlation analysis revealed that correlations in the output spike trains were significantly reduced with respect to the input and decayed to zero for times >2 s (Fig. 5*B*). The power spectrum shows a reduced relative power at low frequencies and is significantly flattened between 0.1 and 1 Hz (Fig. 5*C*).

Similar decorrelation effects were observed with the 1/*f*-type stochastic current injection (Fig. 6). The baseline of the current was adjusted through the injection of constant current so that each neuron had a firing rate of ~10 Hz throughout each 120-s recording session. The 1/*f*-type input exhibits slow variations over time scales of seconds (Fig. 6*A*, *top*). This slow modulation is virtually absent in the neural firing output (Fig. 6*A*, *bottom*). The output's autocorrelation is dramatically suppressed and is near zero for time scales >1 s (Fig. 6*B*). The power spectrum is flattened (whitened) for frequencies <1 Hz (Fig. 6*C*).

The behavior of the recorded cortical neuron is strikingly similar to that of the model endowed with I_{KCa} and I_{KNa} (compare Fig. 6 with Fig. 3). We also compared the histograms of the instantaneous firing rates (calculated as the inverse of the ISIs) for the model and a cortical neuron (Fig. 7). The input amplitude has a Gaussian distribution (Fig. 7*A*). The firing rate histogram for the model neuron without any adaptation current is almost Gaussian-shaped, like the input, except for an additional small peak near zero (corresponding to time periods of relative quiescence; Fig. 7*B*). Adaptation by I_{KCa} increases the probability for low firing rates (peak near 0) and decreases the

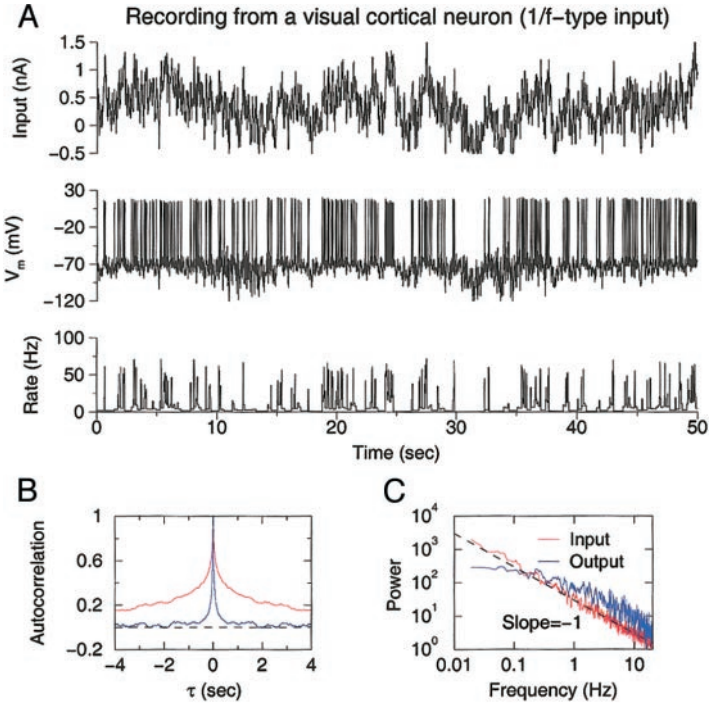

FIG. 6. In vitro intracellular recording from a visual cortical neuron (1/*f*-type input). *A*: neuronal response to a stochastic injected current with 1/*f* type power spectrum (total recording time is 120 s). *Top*: input current; *middle:* membrane potential; *bottom*: instantaneous firing rate. *B*: autocorrelation function shows that the output is greatly decorrelated compared to the input, the autocorrelation function is 0 for time scales >1 s. *C*: power spectrum is flattened for $f < 1$ Hz.

Gaussian-shaped peak at high rates (Fig. 7*C*). The addition of I_{KNa} further altered the firing rate histogram. The peak at high rates virtually disappears, and the peak near zero becomes dominant (Fig. 7*D*). In other words, although most of the time the model neuron fires at low rates, it can occasionally fire transiently at high rates (≤100 Hz). The same characteristic firing rate histogram was found for a real cortical neuron (Fig. 7*E*). The agreement between data and the model provide supporting evidence that intrinsic membrane dynamics of a single neuron in the visual cortex can decorrelate natural-scene-like inputs with long-range temporal correlations.

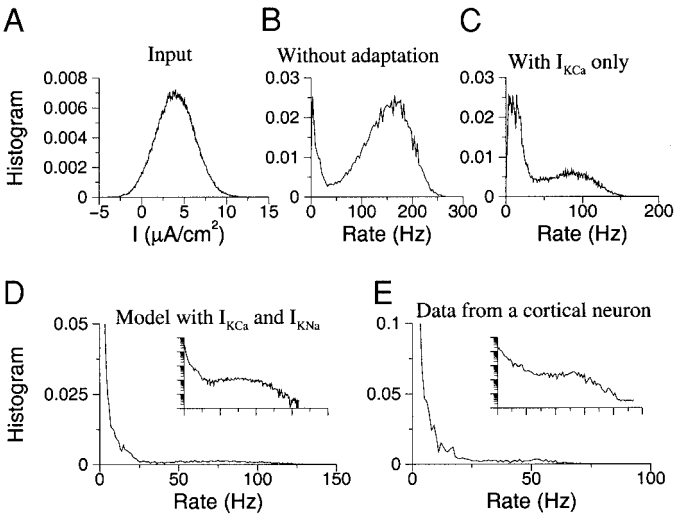

FIG. 7. Distributions of the input intensity and the instantaneous firing rates. The input intensity has a Gaussian distribution (*A*). The instantaneous firing rate histogram of the model neuron without any adaptation current (*B*) and with only I_{KCa} (*C*) show a bimodal distribution. In the presence of both I_{KNa} and I_{KCa}, the model neuron's firing rate histogram shows an exponential function at low rates and a small but broad peak at high rates (*D*). This is similar to the firing-rate histogram from a visual cortical neuron (*E*; the same cell as in Fig. 6).

Relationship between slow hyperpolarization and decorrelation

Because decorrelation is observed with current injection in our slice experiments, it is a single-cell phenomenon. What are the specific membrane mechanisms underlying this decorrelation effect? Evidence indicates that a $[Na^+]_i$-activated K^+ current I_{NaK} plays a large role in the slow hyperpolarization that contributes to adaptation of visual cortical neurons to prolonged inputs (Sanchez-Vives et al. 2000a,b). We attempted to establish a link between the decorrelation effect and slow hyperpolarization, based on the previous observation that the slow hyperpolarization (presumably produced by I_{KNa}) is enhanced in zero calcium solution, compared to control with $[Ca^{2+}]_o = 2$ mM (Sanchez-Vives et al. 2000b). The reason for this enhancement is that under control condition there is a calcium-activated inward current that counteracts I_{KNa}. The removal of calcium eliminates this inward current and unveils a larger slow hyperpolarization (Sanchez-Vives et al. 2000b). Our reasoning is that, if the same adaptation mechanism subserves the decorrelation process, then a stronger decorrelation effect should be observed in zero calcium. We tested this prediction in $n = 5$ cells, with both current pulses and 1/*f*-type stochastic currents. In some cells, we used more than one sample stimuli per cell to increase the number of trials. Neurons show pronounced afterhyperpolarizations (sAHP) following a long (20 s) current injection that is either a single pulse or a train of periodic pulses (at 2 Hz, period of 500 ms, 250 ms on and 250 ms off; Fig. 8). The sAHP is longer lasting in 0 $[Ca^{2+}]_o$ than in control (Fig. 8), consistent with the previous results (Sanchez-Vives et al. 2000b). To quantify the size of sAHP in zero $[Ca^{2+}]_o$ and in control, we calculated the time integral of sAHP divided by the total number of spikes during

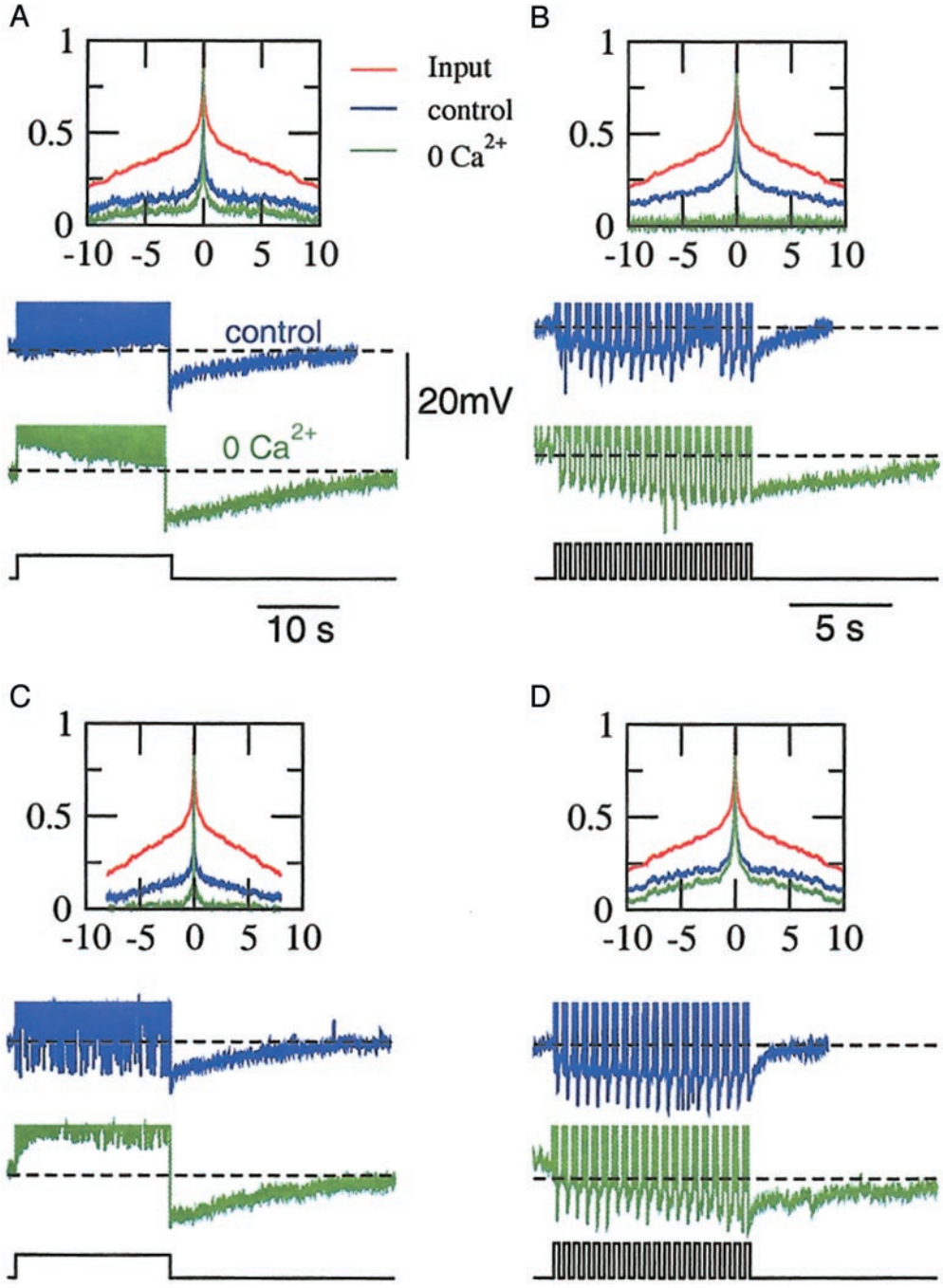

FIG. 8. Increase of slow hyperpolarization and enhancement of decorrelation in 0 $[Ca^{2+}]_o$. *A–D*: 4 different cells are shown. *Top*: autocorrelation function of input (red), output in control medium (blue), and in 0 $[Ca^{2+}]_o$ (green). The autocorrelation is smaller in 0 $[Ca^{2+}]_o$ than in control. *Bottom*: neural response to a long (20 s) current pulse (*A* and *B*) or to a period train of current pulses (*C* and *D*). Note the slow afterhyperpolarization after the input pulse. Slow hyperpolarization is substantially longer-lasting in 0 $[Ca^{2+}]_o$ (green) than in control (blue).

the current injection. As shown in Fig. 9*A*, the sAHP integral per spike is larger in 0 $[Ca^{2+}]_o$ compared to control for all five cells.

When 1/*f*-type correlated stochastic inputs are applied, the autocorrelation of the spiking output is further reduced (decorrelation is more effective) in 0 $[Ca^{2+}]_o$ compared to control. The reduction is very dramatic in some cells (Fig. 8, *B* and *C*) and modest in others (Fig. 8, *A* and *D*). To quantify the decorrelation effect, we calculated the integral of the autocorrelation functions of the input and the output (A_{in} and A_{out}), and used $\rho_{decorr} = A_{out}/A_{in}$ as a decorrelation index. The smaller is ρ_{decorr}, the stronger is the decorrelation effect. In each of the five cells, ρ_{decorr} is substantially smaller in 0 $[Ca^{2+}]_o$ than in control, when the comparison was made with the same 1/*f*-type sample input under the two conditions (Fig. 9*C*). It is important to note that the average firing rate of the neural response to 1/*f*-type input either remains the same or is higher in 0 $[Ca^{2+}]_o$ than in control (Fig. 9*B*). Therefore the stronger decorrelation

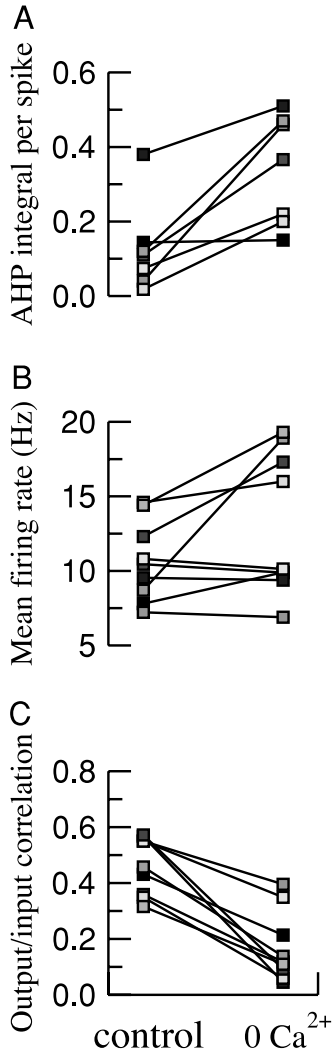

FIG. 9. Increased slow hyperpolarization and enhanced decorrelation in 0 $[Ca^{2+}]_o$. *A*: time integral of afterhyperpolarization per spike is larger in 0 $[Ca^{2+}]_o$ compared to control ($n = 5$, 7 input trials). *B* and *C*: in response to the same sample stochastic 1/*f*-type input, the decorrelation effect is stronger, whereas the overall firing rate is about the same or higher, in 0 $[Ca^{2+}]_o$ than in control ($n = 5$, 8 input trials).

effect cannot be simply attributed to a lower firing rate in 0 $[Ca^{2+}]_o$.

DISCUSSION

Adaptation and gain control of neurons are well-known phenomena and are the subject of many physiological studies over the years. The main novelty of the present work is to demonstrate, using combined computational and electrophysiological methods, that intrinsic spike-frequency adaptation mechanisms can temporally decorrelate inputs at the single neuron level. Based on experimental evidence from V1 pyramidal cells (Sanchez-Vives et al. 2000a,b), we focused on the role in neuronal adaptation of a Na^+-activated K^+ current I_{KNa}. Our main results are: I_{KNa} can dramatically suppress temporal correlations (at time scales >1 s) in the neural firing output when the input is strongly correlated ($1/f^2$ or $1/f$ type) such as in natural-scene stimuli; visual cortical neurons in in vitro slices decorrelate the inputs in the same way as the model; the degree of decorrelation is enhanced at the same time as the size and duration of slow afterhyperpolarization, consistent with the notion that the same ionic channels (e.g., I_{KNa}) underlying slow hyperpolarizations can subserve the decorrelation dynamics of single neurons in the primary visual cortex.

Biophysical mechanisms of slow (seconds) neuronal adaptation

In the primary visual cortex, it has been proposed that contrast adaptation operating at time scales of seconds can arise from short-term depression of afferent synapses (Adorján et al. 1999; Chance et al. 1998). Modeling studies also suggest that short-term synaptic depression provides a candidate mechanism for decorrelation of correlated input spike trains (Goldman et al. 1999, 2002; Matveev and Wang 2000). This proposal is consistent with some in vitro slice experiments (Abbott et al. 1997; Finlayson and Cynader 1995; Tsodyks and Markram 1997; Varela et al. 1997). In an in vivo study of the somatosensory cortex, a rapid depression of thalamocortical synapses (time constant of 0.25–0.32 s) was found to underlie adaptation to whisker stimulation (Chung et al. 2002). However, evidence for slow (time constant of seconds) synaptic depression in the intact brain is still lacking. Recently Sanchez-Vives et al. (2000a,b) discovered that slow adaptation during prolonged visual stimuli depends on the intrinsic activation of ionic conductances, such as I_{KNa}. These and other (Carandini and Fester 1997) studies did not find a consistent decrease in visually evoked synaptic barrages following adaptation; a finding that is inconsistent with a strong role for synaptic depression in adaptation. In support of this view, we show here that a cortical pyramidal cell model endowed only with I_{KNa} and I_{KCa} can reproduce adaptation to high-amplitude sinusoidal input mimicking a high-contrast visual stimulus (Fig. 1).

Further experiments are needed to quantitatively test our model and the role of I_{KNa} in adaptation. One possibility is to use synthetic Na^+ buffers, which should prevent $[Na^+]_i$ accumulation and hence block I_{KNa} activation (K. Svoboda, personal communication). Another critical issue is to determine the $[Na^+]_i$ dynamics in V1 pyramidal cells: what is the $[Na^+]_i$ influx per spike? To what level can $[Na^+]_i$ accumulate during a long-lasting stimulation? How fast is the Na^+/K^+ exchange? In the model, assuming that the baseline $[Na^+]_i$ is 8 mM (Galvan et al. 1984; Grafe et al. 1982), and that $[Na^+]_i$ is increased by 100 μM per spike, the $[Na^+]_i$ level typically reaches 15–20 mM after long-lasting (many tens of seconds) neural discharges at an average rate of 20 Hz. In a recent experiment, Rose et al. (1999) used Na^+ indicator dye SBFI and two-photon imaging to measure intracellular Na^+ concentration evoked by action potentials in dendrites and spines of hippocampal CA1 pyramidal cells. They found that the $[Na^+]_i$ signal can integrate the spike activity, because it has slow kinetics (time constant of several seconds). The spike-triggered $[Na^+]_i$ transients reached values of 1, 2, and 4 mM for a train of 5, 10, and 20 spikes, respectively. Therefore the $[Na^+]_i$ transient is $\sim$200 μM per action potential in the fine dendrites and spines. Because this rate of accumulation is twice the value used in our model, we expect that in pyramidal cell's dendrites, the $[Na^+]_i$ can reach 15–20 mM after tens of seconds of neural discharges at an average rate of 10 Hz. It would be interesting to test directly our prediction by Na^+ imaging of visual cortical

neurons during prolonged discharges as in the contrast adaptation experiments.

Moreover, it would be important to know the precise spatial site of $[Na^+]_i$ accumulation with respect to the location of I_{KNa}. For example, an increase in intracellular $[Na^+]_i$ may be tightly localized in the submembrane space and reach levels high enough to activate I_{KNa} (Koh et al. 1994). Moreover, due to the difference in the surface/volume ratio, activity-induced $[Na^+]_i$ accumulation could vary widely at different somatic and dendritic compartments of a single neuron (Qian and Sejnowski 1989). Therefore the spatial distribution of I_{KNa} across the somatodendritic membrane is important to be determined experimentally. It is conceivable that hyperpolarizations of different portions of a neuron's dendritic tree may result from localized entry of Ca^{2+} and Na^+ and activation of nearby I_{KCa} and I_{KNa} channels. This may serve to temporally decorrelate inputs to restricted dendritic segments, while leaving others segments less affected.

Finally, it would also be interesting to explore additional or alternative ionic mechanisms for neuronal adaptation in the cortex and other brain structures. In retinal ganglion neurons, slow adaptation (Baccus and Meister 2002; Chander and Chichilnisky 2001; Shapley 1997; Shapley and Victor 1978; Simirnakis et al. 1997) may be related to properties of Na^+ channels in these cells (Kim and Rieke 2001, 2003), or/and reflect cellular mechanisms upstream in bipolar neurons (Brown and Masland 2001; Rieke 2001). It would be interesting to test experimentally whether such adaptation mechanisms also subserve input decorrelation in retinal neurons.

Decorrelation at the single-cell level

In our model, when driven by stochastic inputs with long-range temporal correlations, I_{KCa} and I_{KNa} remove correlations in the spiking output at different time scales (10–100 ms and 1–10 s, respectively). In the output power spectrum, at <1 Hz the power is reduced to a plateau level (is whitened) by I_{KNa}, while I_{KCa} results in a flattening of the power-frequency function at frequencies between 1 and 10 Hz. We noticed that when the output firing rate is very low, decorrelation could be a trivial consequence of the fact that most of the time the cell membrane is subthreshold, the consecutive spikes are separated by long times compared to the input correlation time, so that most of the correlation information in the input is lost. This happens when the output firing rate is roughly lower than the inverse of the input correlation time ($<$1–2 Hz with an input correlation time of 2 s). For this reason, both for model simulations and experimental studies, we always made sure to depolarize the cell with a baseline current when injected with correlated current, so that the cells fire spikes throughout the stimulation with a relatively high mean firing rate (10–20 Hz generally).

Interestingly, we found that visual cortical neurons in vitro show similar decorrelation properties as the model (compare Figs. 5 and 6 for data with Figs. 2 and 3 for the model). The distribution of instantaneous firing rates is also similar for the visual cortical cell and the model (Fig. 7): it is roughly exponential at low rates, but there is a second broad peak at larger firing rates ($\sim$50–80 Hz). We attempted to further establish the link between the slow hyperpolarization and the decorrelation effect by comparing the neuronal behavior in zero-calcium bath solution with that in control. We confirmed the previous observation (Sanchez-Vives et al. 2000b) that for a given cell, the slow hyperpolarization after spiking activity is stronger and longer lasting in zero calcium than in control. Furthermore in response to the exactly same sample of stochastic correlated input, the decorrelation effect was stronger in zero calcium than in control (Figs. 8 and 9). This result lends support to the idea that the same ion channel mechanism responsible for the slow hyperpolarization also underlies the decorrelation process of temporally correlated stochastic inputs. However, our results only show that the two effects increase in a correlated way, and we do not have direct proof for the hypothesized role of I_{KNa} in the observed decorrelation phenomenon at the single-cell level.

It is worth noting that an adaptation mechanism removes correlations most effectively at time scales comparable to its intrinsic time constant. Therefore with I_{KNa} and I_{KCa} a neuron's output can still show large autocorrelations at time scales shorter than a few hundreds of milliseconds. The adaptation mechanism of redundancy reduction is thus compatible with the fact that cortical neuronal spike trains do show autocorrelations at time scales ranging from one to hundreds of milliseconds (for a review, see Singer and Gray 1995).

We have not addressed the question of whether the filter functions of cortical neurons are optimally designed. That is, the kinetics and strength of adaptation ionic mechanisms might have been optimized, through biological evolution, for redundancy reduction of the kind of natural stimuli that the animal encounters in daily life (Atick 1992). Specifically, one could ask whether the calcium- and sodium-activated potassium currents decorrelate $1/f$ *and* $1/f^2$ stimuli better than inputs with other statistic properties. However, what it means to be "optimal" remains to be clarified. Indeed, most likely, complete whitening of stimulus by decorrelation is not desirable because probability distributions of stimuli may themselves be used for neural representation of the sensory world in the brain (Barlow 2001; Rao et al. 2002).

Adaptation and decorrelation in the V1 network

Computational theories suggest that in the mammalian visual system, natural inputs are decorrelated spatially at the level of the retina (Atick 1992) and temporally in the lateral geniculate nucleus (LGN) (Dong and Atick 1995b) so that signals that arrive in the visual cortex are encoded in an efficient form. In support of this proposal, physiological studies show that in response to natural time-varying images (movies), neurons in the cat LGN remove temporal correlations at the time scales of 50–300 ms, and the output power spectrum is whitened in the frequency range of 3–15 Hz (Dan et al. 1996). The underlying biophysical mechanism could be, at least partly, intrinsic membrane properties of the LGN relay cells. Indeed these cells are known to display burst discharges due to a T-type calcium ion current; this burst activity can remove temporal correlations in an input at the time scale of $\sim$100 ms (Kepecs et al. 2002). However, LGN cells fire bursts only under certain conditions (including sodium pentothal anesthesia as in the experiment of Dan et al. 1996); their propensity of burst discharge during waking states remains a matter of debate (Sherman 2001). Therefore it is still unclear whether temporal

decorrelation primarily takes place in the LGN during animal's natural behaviors.

Here we hypothesize that temporal decorrelation of inputs is to a large extent accomplished in the primary visual cortex by the same mechanisms responsible for the contrast adaptation. Synaptic depression can temporally decorrelate inputs in a synapse-specific manner and at the time scale of hundreds of milliseconds (on a similar time scale as fast intrinsic adaptation through I_{KCa}); whereas intrinsic membrane dynamics mediated by I_{KNa} operate at a more global level of the neural activity and at a slower time scale of seconds. To explore this proposal computationally, it will be necessary to extend our investigation to pattern adaptation in a V1 network model, that takes into account short-term synaptic depression (Adorján et al. 1999; Somers et al. 1998) and slow spike-frequency adaptation by I_{KNa} in single neurons. Network modeling would enable us to investigate the mechanisms for pattern adaptation and whether the same mechanisms can remove spatiotemporal correlations in the natural-scene inputs thereby performing redundancy reduction in both space and time. Experimentally, our proposal could be tested by physiological studies of V1 neurons in response to natural time-varying stimulations (such as movies). Further experimental and theoretical studies will lead to the elucidation of specific cellular mechanisms of adaptation and redundancy reduction processes in the visual cortex.

APPENDIX: QUALITATIVE EXPLANATION OF POWER SPECTRUM WHITENING BY AN ADAPTATION CURRENT

To understand whitening or flattening of the neural output power spectrum within a frequency range, let us consider a linear model of adaptation, $I_{adap} = G_{adap}X$ *where* $X = [Ca^{2+}]_i$ or $[Na^+]_i$, if $I_{adap} = I_{KCa}$ or I_{KNa}, respectively. Furthermore, assume that X obeys a linear kinetic equation

$$\frac{dX}{dt} = \alpha \sum_i \delta(t - t_i) - \frac{X}{\tau_X} \simeq \alpha r(t) - X/\tau_X \qquad (A1)$$

where the spike train $\sum_i \delta(t - t_i)$ is replaced by the instantaneous firing rate, which is a valid approximation as long as τ_X is significantly longer than a typical ISI. The parameter α is the X influx per spike, and τ_X is the time constant ($\sim$100 ms for $[Ca^{2+}]_i$, and $\sim$10 s for $[Na^+]_i$). Note that although the Na^+ extrusion process is highly nonlinear, the present discussion assuming a linear kinetics is nevertheless instructive.

Suppose that in response to a time-varying stochastic input current I, the neuron's output firing rate is given by $r(t) = \beta I_{tot}$, where $I_{tot} = I - I_{adap}$, and the firing threshold I_{th} is absorbed in I. Therefore, $r(t) \simeq \beta[I(t) - I_{adap}(t)]$. Inserting this expression into *Eq. A1* we have

$$\frac{dX}{dt} = \alpha\beta I(t) - (\alpha\beta G_{adap} + 1/\tau_X)X = \alpha\beta I(t) - X/\tau_{adap} \qquad (A2)$$

where we define the adaptation time constant τ_{adap} as

$$1/\tau_{adap} = \alpha\beta G_{adap} + 1/\tau_X \qquad (A3)$$

Due to the additional term $\alpha\beta G_{adap}$, τ_{adap} is typically much shorter than τ_X (see also Liu and Wang 2001; Wang 1998).

The solution of *Eq. A2* yields

$$X(t) = \int_0^t \alpha\beta I(t')e^{-(t-t')/\tau_{adap}}dt' = \alpha\beta I * K \qquad (A4)$$

where the kernel of the convolution is

$$K(t) = \begin{cases} e^{-t/\tau_{adap}} & \text{if } t \geq 0 \\ 0 & \text{otherwise} \end{cases} \qquad (A5)$$

The Fourier transforms of the kernel K, X, and r are as follows

$$F(K) = \frac{-1}{i\omega - \dfrac{1}{\tau_{adap}}} \qquad (A6)$$

$$F(X) = \alpha\beta F(I)F(K) \qquad (A7)$$

$$F(r) = \beta[F(I) - G_{adap}F(X)] = \beta F(I)[1 - G_{adap}\alpha\beta F(K)] \qquad (A8)$$

Therefore the output power spectrum $S_O = |F(r)|^2$ can be expressed as a function of the input power $S_I = |F(I)|^2$

$$S_O(\omega) = S_I(\omega)\beta^2 \frac{\omega^2 + (1/\tau_X)^2}{\omega^2 + (1/\tau_{adap})^2} \qquad (A9)$$

Without adaptation, it is easy to show that

$$S_O(\omega) = \beta^2 S_I(\omega) \qquad (A10)$$

Thus the presence of I_X introduces a temporal kernel that convolves with the input to produce the output. This leads to an additional multiplicative factor for the output power spectrum

$$\frac{\omega^2 + (1/\tau_X)^2}{\omega^2 + (1/\tau_{adap})^2} \qquad (A11)$$

where τ_{adap} is typically much smaller than τ_X. At low frequencies $\omega \ll 1/\tau_X$, the additional factor is $\sim(\tau_{adap}/\tau_X)^2 \ll 1$. (Note that at very low frequencies, this analysis is no longer valid because the assumption that the firing is faster than the X dynamics is no longer correct.) In the frequency range $1/\tau_X \ll \omega \ll 1/\tau_{adap}$, this factor is $\sim\omega^2$. At very high frequencies, this factor is 1, reflecting the fact that the slow adaptation current has no effect as expected. Thus spike-frequency adaptation provides a high-pass filter in the intermediate frequency range $1/\tau_X \ll \omega \ll 1/\tau_{adap}$. If $I(t)$ is a temporally correlated input with a power spectrum $S_I(\omega) \sim \omega^{-2}$, the output spike train is decorrelated; the power spectrum is $S_O(\omega) \sim S_I\omega^2 \sim$ const. Thus S_O would be almost flat (whitened) and behave like white noise for $1/\tau_X \ll \omega \ll 1/\tau_{adap}$.

We thank S. Nelson and N. Brunel for a critical reading of this paper.

This work was supported by National Science Foundation, the Alfred P. Sloan Foundation, and the Swartz Foundation to X.-J. Wang; by Grants GV00-138-3 (Generalitat Valenciana) and PM98-0102-CO2-01 (DGCYT, Spain) to M.V. Sanchez-Vives; and by National Eye Institute R01 to D.A. McCormick.

REFERENCES

Abbott LF, Varela JA, Sen K, and Nelson SB. Synaptic depression and cortical gain control. *Science* 275: 220–224, 1997.

Adorján P, Piepenbrock C, and Obermayer K. Contrast adaptation and info-max in visual cortical neurons. *Rev Neurosci* 10: 181–200, 1999.

Aghajanian GK and Rasmussen K. Intracellular studies in the facial nucleus illustrating a simple new method for obtaining viable motor neurons in adult rat brain slices. *Synapse* 3: 331–338, 1989.

Ahmed B, Allison JD, Douglas RJ, and Martin KAC. An intracellular study of the contrast-dependence of neuronal activity in cat visual cortex. Cereb Cortex 7: 559–570, 1997.

Atick JJ. Could information theory provide an ecological theory of sensory processing? *Network* 3: 213–251, 1992.

Attneave F. Some informational aspects of visual perception. *Pysch Rev* 61: 183–193, 1954.

Baccus SA and Meister M. Fast and slow contrast adaptation in retinal circuitry. *Neuron* 36: 909–919, 2002.

Baddeley R, Abbott LF, Booth MC, Sengpiel F, Freeman T, Wakeman EA, and Rolls ET. Responses of neurons in primary and inferior temporal visual cortices to natural scenes. *Proc R Soc Lond B Biol Sci* 264: 1775–1783, 1997.

Barlow HB. Possible principles underlying the transformations of sensory messages. In: *Sensory Communication,* edited by Rosenblith WA. Cambridge, MA: MIT Press, 1961, p. 217–234.

Barlow HB. A theory about the functional role and synaptic mechanism of visual after-effects. In: *Vision: Coding and Efficiency,* edited by Blakemore C. Cambridge, UK: Cambridge University Press, 1990.

Barlow HB. Redundancy reduction revisited. *Network Comput Neural Systems* 12: 241–253, 2001.

Barlow HB and Foldiak P. Adaptation and decorrelation in the cortex. In: *The Computing Neuron,* edited by Durbin R, Miall C, and Mitchison G. New York: Addison-Wesley, 1989, p. 454–472.

Bell AJ and Sejnowski TJ. The "independent components" of natural scenes are edge filters. *Vision Res* 37: 3327–3338, 1997.

Bischoff U, Vogel W, and Safronov BV. Na^+-activated K^+ channels in small dorsal root ganglion neurons of rat. *J Physiol* 510: 743–754, 1998.

Blakemore CB and Campbell FW. On the existence of neurones in the human visual system selectively sensitive to the orientation and size of retinal images. *J Physiol* 203: 237–260, 1969.

Brenner N, Bialek W, and de Ruyter van Steveninck R. Adaptive rescaling maximizes information transmission. *Neuron* 26: 695–702, 2000.

Brown SP and Masland RH. Spatial scale and cellular substrate of contrast adaptation by retinal ganglion cells. *Nat Neurosci* 4: 44–51, 2001.

Carandini M and Ferster D. A tonic hyperpolarization underlying contrast adaptation in cat visual cortex. *Science* 276: 949–952, 1997.

Carandini M, Movshon JA, and Ferster D. Pattern adaptation and cross-orientation interactions in the primary visual cortex. *Neuropharmacology* 37: 501–511, 1998.

Chance FS, Nelson SB, and Abbott LF. Synaptic depression and the temporal response characteristics of V1 cells. *J Neurosci* 18: 4785–4799, 1998.

Chander D and Chichilnisky EJ. Adaptation to temporal contrast in primate and salamander retina. *J Neurosci* 21: 9904–9916, 2001.

Chung S, Li X, and Nelson SB. Short-term depression at thalamocortical synapses contributes to rapid adaptation of cortical sensory responses in vivo. *Neuro* 34: 437–446, 2002.

Dan Y, Atick JJ, and Reid RC. Efficient coding of natural scenes in the lateral geniculate nucleus: experimental test of a computational theory. *J Neurosci* 16: 3351–3362, 1996.

Dong DW and Atick JJ. Statistics of natural time-varying images. *Network Comput Neural Systems* 6: 345–358, 1995a.

Dong DW and Atick JJ. Temporal decorrelation: a theory of lagged and nonlagged responses in the lateral geniculate nucleus. *Network Comput Neural Systems* 6: 159–178, 1995b.

Dragoi V, Sharma J, and Sur M. Adaptation-induced plasticity of orientation tuning in adult visual cortex. *Neuron* 28: 287–298, 2000.

Dryer SE. Na^+-activated K^+ channels: a new family of large-conductance ion channels. *Trends Neurosci* 17: 155–160, 1994.

Egan TM, Dagan D, Kupper J, and Levitan IB. Properties and rundown of sodium-activated potassium channels in rat olfactory bulb neurons. *J Neurosci* 12: 1964–1976, 1992a.

Egan TM, Kupper J, and Levitan IB. Na^+-activated K^+ channels are widely distributed in rat CNS and Xenopus ocytes. *Brain Res* 584: 319–321, 1992b.

Ermentrout B. Linearization of F-I curves by adaptation. *Neural Comput* 10: 1721–1929, 1998.

Fain GL. *Molecular and Cellular Physiology of Neurons.* Cambridge, MA: Harvard Univ. Press, 1999.

Fairhall AL, Lewen GD, Bialek W, de Ruyter Van Steveninck RR. Efficiency and ambiguity in an adaptive neural code. *Nature* 412: 787–792, 2001.

Field DJ. What is the goal of sensory coding? *Neural Comput* 6: 559–601, 1994.

Finlayson PG and Cynader MS. Synaptic depression in visual cortex tissue slices: an in vitro model for cortical neuron adaptation. *Exp Brain Res* 106: 145–155, 1995.

Gabbiani F and Koch C. Principles of spike train analysis. In: *Methods in Neuronal Modeling: From Synapses to Networks* (2nd ed.) edited by Koch C and Segev I. Cambridge, MA: MIT Press, 1998, p. 313–360.

Galvan M. Dorge A, Beck F, and Rick R. Intracellular electrolyte concentrations in rat sympathetic neurones measured with an electron microprobe. Pflugers Arch 400: 274–279, 1984.

Goldman MS, Maldonado P, and Abbott LF. Redundancy reduction and sustained firing with stochastic depressing synapses. *J Neurosci* 22: 584–591, 2002.

Goldman MS, Nelson SB, and Abbott LF. Decorrelation of spike trains by synaptic depression. Neurocomputing 26/27: 147–153, 1999.

Grafe P, Rimpel J, and Reddy MM. Changes of intracellular sodium and potassium ion concentrations in frog spinal motoneurons induced by repetitive synaptic stimulation. *Neuroscience* 7: 2113–2120, 1982.

Greenlee MW, Georgeson MA, Magnussen S, and Harris JP. The time course of adaptation to spatial contrast. *Vision Res* 31: 223–236, 1991.

Greenlee MW and Heitger F. The functional role of contrast adaptation. *Vision Res* 28: 791–797, 1988.

Helmchen F, Imoto K, and Sakmann B. Ca^{2+} buffering and action potential-evoked Ca^{2+} signaling in dendrites of pyramidal neurons. *Biophys J* 70: 1069–1081, 1996.

Hodgkin AL and Huxley AF. A quantitative description of membrane current and its application to conduction and excitation in nerve. *J Physiol* 117: 500–544, 1952.

Jaffe DB, Johnston D, Lasser-Ross N, Lisman JE, Miyakawa H, and Ross WN. The spread of Na+ spikes determines the pattern of dendritic Ca2+ entry into hippocampal neurons. *Nature* 357: 244–256, 1992.

Kameyama M, Sato M, Shibasaki R, Matsuda T, and Irisawa H. Intracellular Na^+ activates a K^+ channel in mammalian cardiac cells. *Nature* 309: 354–356, 1984.

Kepecs A, Wang X-J, and Lisman J. Burst neurons signal input slope. *J Neurosci* 22: 9053–9062, 2002.

Kim KJ and Rieke F. Temporal contrast adaptation in the input and output signals of salamander retinal ganglion cells. *J Neurosci* 21: 287–299, 2001.

Kim KJ and Rieke F. Slow Na^+ inactivation and variance adaptation in salamander retinal ganglion cells. *J Neurosci* 23: 1506–1516, 2003.

Koh DS, Jonas P, and Vogel W. Na^+-activated K^+ channels localized in the nodal region of myelinated axons of *Xenopus. J Physiol* 479:183–197, 1994.

Laughlin SB. A simple coding procedure enhances a neurons information capacity. *Z Naturforsch* 36: 910–912, 1981.

Li YX, Bertran R, and Rinzel J. Modeling *N*-methyl-D-aspartate-induced bursting in dopamine neurons. *Neuroscience* 71: 397–410, 1996.

Liu YH and Wang X-J. Spike-frequency adaptation of a generalized integrate-and-fire model neuron. *J Comput Neurosci* 10: 25–45, 2001.

Maffei L, Fiorentini A, and Bisti S. Neural correlate of perceptual adaptation to gratings. *Science* 182: 1036–1038, 1973.

Matveev V and Wang X-J. Differential short-term synaptic plasticity and transmission of complex spike trains: to depress or to facilitate? *Cereb Cortex* 10: 1143–1153, 2000.

Movshon JA and Lennie P. Pattern-selective adaptation in visual cortical neurones. *Nature* 278: 850–852, 1979.

Nelson SB. Temporal interactions in the cat visual system. *J Neurosci* 11: 344–380, 1991.

Ohzawa I, Sclar G, and Freeman RD. Contrast gain control in the cat's visual system. *J Neurophysiol* 54: 651–667, 1985.

Olshausen BA and Field DJ. Emergence of simple-cell receptive field properties by learning a sparse code for natural images. *Nature* 381: 607–609, 1996.

Pinsky P and Rinzel J. Intrinsic and network rhythmogenesis in a reduced Traub model for CA3 neurons. *J Comput Neurosci* 1: 39–60, 1994.

Qian N and Sejnowski TJ. An electro-diffusion model for computing membrane potentials and ionic concentrations in branching dendrites, spines and axons. *Biol Cybern* 62: 1–15, 1989.

Rao RP, Olshausen BA, and Lewicki MS. *Probabilistic Models of the Brain.* Cambridge, MA: MIT Press, 2002.

Rieke F. Temporal contrast adaptation in salamander bipolar cells. *J Neurosci* 21: 9445–9454, 2001.

Rose CR, Kovalchuk Y, Eilers J, and Konnerth A. Two-photon Na+ imaging in spines and fine dendrites of central neurons. *Pflugers Arch* 439: 201–207, 1999.

Rose CR and Ransom BR. Regulation of intracellular sodium in cultured rat hippocampal neurons. *J Physiol* 499: 573–587, 1997.

Ruderman DL. The statistics of natural images. *Network Comput Neural Syst* 5: 517–548, 1994.

Ruderman DL and Bialek W. Statistics of natural images: scaling in the woods. *Physical Rev Lett* 73: 814–817, 1994.

Sanchez-Vives MV, Nowak LG, and McCormick DA. Membrane mechanisms underlying contrast adaptation in cat area 17 in vivo. *J Neurosci* 20: 4267–4285, 2000a.

Sanchez-Vives MV, Nowak LG, and McCormic DA. Cellular mechanisms of long-lasting adaptation in visual cortical neurons in vitro. *J Neurosci* 20: 4286–4299, 2000b.

Schwindt RC, Spain WJ, and Crill WE. Long-lasting reduction of excitability by a sodium-dependent potassium current in cat neocortical neurons. *J Neurophysiol* 61: 233–244, 1989.

Schwindt RC, Spain WJ, Foehring RC, Chubb MC, aned Crill WE. Slow conductances in neurons from cat sensorimotor cortex in vitro and their role in slow excitability changes. *J Neurophysiol* 59: 450–467, 1988.

Sclar G, Ohzawa I, and Freeman RD. Contrast gain control in the kitten's visual system. *J Neurophysiol* 54: 668–673, 1985.

Shapley R. Retinal physiology: adapting to the changing scene. *Curr Biol* 7: R421–423, 1997.

Shapley R and Victor JD. The effect of contrast on the transfer properties of cat retinal ganglion cells. *J Physiol* 285: 275–298, 1978.

Sherman SM. Tonic and burst firing: dual modes of thalamocortical relay. *Trends Neurosci* 24: 122–126, 2001.

Simoncelli EP and Olshausen BA. Natural image statistics and neural representation. *Annu Rev Neurosci* 24: 1193–1216, 2001.

Singer W and Gray CM. Visual feature integration and the temporal correlation hypothesis. *Annu Rev Neurosci* 18: 555–586, 1995.

Smirnakis SM, Berry MJ, Warland DK, Bialek W, and Meister M. Adaptation of retinal processing to image contrast and spatial scale. *Nature* 386: 69–73, 1997.

Somers DC, Todorov EV, Siapas AG, Toth LJ, Kim DS, and Sur M. A local circuit approach to understanding integration of long-range inputs in primary visual cortex. *Cereb Cortex* 8: 204–217, 1998.

Srinivasan MV, Laughlin SB, and Dubs A. Predictive coding: a fresh view of inhibition in the retina. J R Soc Lond B Biol Sci 216: 427–459, 1982.

Tsodyks M and Markram H. The neural code between neocortical pyramidal neurons depends on neurotransmitter release probability. *Proc Natl Acad Sci USA* 94: 719–723, 1997.

Varela JA, Sen K, Gibson J, Fost J, Abbott LF, and Nelson SB. A quantitative description of short-term plasticity at excitatory synapses in layer 2/3 of rat primary visual cortex. *J Neurosci* 17: 7926–2940, 1997.

van Hateren JH. Processing of natural time series of intensities by the visual system of the blowfly. *Vision Res* 37: 3407–3416, 1997.

van Hateren JH and van der Schaaf A. Temporal properties of natural scenes. *IS&T/SPIE Proceedings* 2657: 139–143, 1996.

Vidyasagar TR. Pattern adaptation in cat visual cortex is a cooperative phenomenon. *Neurosci* 36: 175–179, 1990.

Vinje WE and Gallant JL. Sparse coding and decorrelation in primary visual cortex during natural vision. *Science* 287: 1273–1276, 2000.

Wainwright MJ. Visual adaptation as optimal information transmission. *Vis Res* 39: 3960–3974, 1999.

Wang X-J. Calcium coding and adaptive temporal computation in cortical pyramidal neurons. *J Neurophysiol* 79: 1549–1566, 1998.